Biopolymer-based capillary suspensions

Influence of particle properties on network formation

Feichtinger, Annika; Jarray, Ahmed; Bouwman, Wim G.; Duif, Chris P.; Valverde-Ayllon, Maria C.; Heerkens, Karlijn; Rooijakkers, Renee; Landman, Jasper; Scholten, Elke

DOI
10.1016/j.foodhyd.2025.111061

Publication date
2025

Document Version
Final published version

Published in
Food Hydrocolloids

Citation (APA)
Feichtinger, A., Jarray, A., Bouwman, W. G., Duif, C. P., Valverde-Ayllon, M. C., Heerkens, K., Rooijakkers, R., Landman, J., & Scholten, E. (2025). Biopolymer-based capillary suspensions: Influence of particle properties on network formation. *Food Hydrocolloids*, *163*, Article 111061. https://doi.org/10.1016/j.foodhyd.2025.111061

Food Hydrocolloids 163 (2025) 111061

Contents lists available at ScienceDirect

Food Hydrocolloids

journal homepage: www.elsevier.com/locate/foodhyd

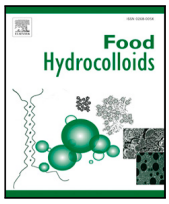

Biopolymer-based capillary suspensions: Influence of particle properties on network formation

Annika Feichtinger [a], Ahmed Jarray [a], Wim G. Bouwman [b], Chris P. Duif [b], Maria C. Valverde-Ayllon [a], Karlijn Heerkens [a], Renee Rooijakkers [a], Jasper Landman [a], Elke Scholten [a,*]

[a] Physics and Physical Chemistry of Foods, Wageningen University and Research, Bornse Weilanden 9, Wageningen, 6708 WG, The Netherlands
[b] Faculty of Applied Sciences, Delft University of Technology, Mekelweg 15, Delft, 2629 JB, The Netherlands

ARTICLE INFO

Keywords:
Capillary systems
Oleogels
Biopolymeric particles
Water-absorption capacity
SESANS
Water distribution

ABSTRACT

Capillary suspensions are unique materials, in which the rheological properties can be tuned by controlling the particle network through capillary interactions. To gain insights into the influence of particle properties on the network formation and accompanying gel strength for water-absorbing, biopolymeric particles, protein particles of two different sizes and water absorption capacities (WACs) were prepared. Utilizing SESANS, we describe a novel approach towards detecting changes in water distribution between and within particles. While effects of WAC seemed to be overpowered by concurrent variations in surface roughness, a larger particle size or lower roughness led to a lower initial gel strength and a subsequent much larger relative increase in gel strength upon water addition. Even though similar maximum gel strengths were obtained, indicating that particle properties had a comparably small influence once capillary forces dominated the systems, particle size played a critical role for network collapse with increasing particle clustering at larger water volumes. The results pinpoint subsequent knowledge gaps in the existing literature and demonstrate the tunability of biopolymer-based capillary suspensions over a wide gel strength range by adjustment of particle properties. These insights offer exciting opportunities for application of capillary-force controlled systems in the food, pharmaceutical and cosmetic industries.

1. Introduction

Although capillary suspensions have received increasing scientific attention only over the past decade, such systems have already been used for centuries, for example for adjusting the thickness of oil paints by addition of egg yolk during the Renaissance period by Masters such as Leonardo da Vinci (Ranquet et al., 2023). In this case, egg yolk acts as an immiscible secondary liquid, bridging the pigments suspended in oil together, which leads to drastic changes of the material properties. The capillary bridge formation of the secondary liquid leads to a strong attractive force between the suspended particles, thereby inducing the formation of a percolating network or considerably increasing the strength of an existing network. The capillary force induced by the pendular liquid bridge between two smooth particles in contact with each other (in air) is determined by their radius r, the surface tension Γ of the liquid, and the wetting angle θ between the particle and liquid as (Koos, Johannsmeier, Schwebler, & Willenbacher, 2012):

$$F_c = 2\pi r \Gamma \cos\theta \quad (1)$$

Depending on the wettability of the particles, capillary suspensions can form in either the pendular or capillary state. The pendular state, in which particles are connected by concave bridges, occurs when the secondary liquid preferentially wets the particles ($\theta < 90°$). The capillary state occurs when the secondary liquid does not preferentially wet the particles ($\theta > 90°$), leading to particles clustering around small volumes of the secondary liquid to shield it from the bulk liquid. These enhanced attractive interactions between particles due to the formation of capillary bridges then result in the transition from liquids to solid gels, or from weak to strong gels (Dittmann & Willenbacher, 2014; Koos et al., 2012).

Knowledge on how capillary interactions alter the rheological properties serves as a tool to tune the properties of existing materials, as well as to develop new materials. Most research on capillary suspensions has been performed with synthetic particles, such as silica particles or

* Corresponding author.
E-mail addresses: annika.feichtinger@wur.nl (A. Feichtinger), ahmed.jarray@wur.nl (A. Jarray), w.g.bouwman@tudelft.nl (W.G. Bouwman), c.p.duif@tudelft.nl (C.P. Duif), jasper.landman@wur.nl (J. Landman), elke.scholten@wur.nl (E. Scholten).

https://doi.org/10.1016/j.foodhyd.2025.111061
Received 8 July 2024; Received in revised form 21 October 2024; Accepted 7 January 2025
Available online 14 January 2025

glass beads (Allard et al., 2022; Bossler & Koos, 2016; Bossler, Maurath, Dyhr, Willenbacher, & Koos, 2018; Bossler, Weyrauch, Schmidt, & Koos, 2017; Domenech & Velankar, 2015; Jarray, Feichtinger, & Scholten, 2022; Koos et al., 2012; Koos & Willenbacher, 2011), aluminum oxide (Bossler et al., 2018, 2017; Dittmann & Willenbacher, 2014) or calcium carbonate (Bossler et al., 2017; Koos et al., 2012; Koos & Willenbacher, 2011). Next to paints and inks, common applications include for example lithium-ion batteries, by adjusting the rheology of an electrode slurry, and porous ceramics, where stabilization via capillary forces enables the formation of a porous template structure (Koos, 2014).

Capillary suspensions may also be beneficial in the food and pharmaceutical industry. However, for such materials, synthetic particles are less suitable, and particles consisting of biopolymeric material are desired. For example, starch, cocoa (Hoffmann, Koos, & Willenbacher, 2014), protein (de Vries, Jansen, van der Linden, & Scholten, 2018; Fysun, Nöbel, Loewen, & Hinrichs, 2018; Wang et al., 2022), soy fiber (Li et al., 2023), wheat middlings (Pirozzi & Donsì, 2023; Pirozzi, Posocco, & Donsì, 2023), or cellulose particles (Fuhrmann, Powell, & Rousseau, 2023; Gao et al., 2023; Pirozzi & Donsì, 2023) have been utilized for the formation of capillary suspensions. Biopolymeric particles may behave very differently from synthetic particles, as their properties can differ substantially. Unlike synthetic particles, biopolymeric particles can take up large amounts of water and swell. In addition, such particles are often less defined in terms of shape and size. Particle properties have a large influence on the rheological behavior of the final gels, as they determine both the interactions between particles (de Vries, 2017; Feichtinger et al., 2022) and the liquid bridge formation (Bindgen, Allard, & Koos, 2022). In research utilizing biopolymeric particles, the influence of absorption capacity or other particle properties has not yet been systematically studied.

In research with porous silica particles, it has been shown that the distribution of water, which is either absorbed within the porous particles or remains between the particles, indeed influences the final gel strength. A network can only form when a sufficient amount of secondary liquid is still present between the particles (Bindgen et al., 2022; Bossler & Koos, 2016). In addition, particle porosity was found to strongly influence the dependence of the obtained capillary structures on the contact angle, evidenced by a transition from a pendular to a capillary state at higher apparent contact angles for porous particles (Bossler & Koos, 2016). Similarly, differences in surface roughness influence the amount of secondary liquid necessary to form water bridges, as well as the contact angle and subsequently strength of the capillary force. For rougher surfaces, more secondary liquid is needed for bridge formation, as first surface asperities need to be filled (Allard et al., 2022; Nguyen, Zhao, Millet, & Selvadurai, 2021).

Understanding of the influence of such particle properties on rheological behavior is especially relevant for biopolymeric particles, which, as mentioned, by nature do not only vary in size, but also absorb water and have an irregular shape. Particularly for water absorption, a distinct influence on the mechanisms of capillary bridge formation is obvious. Available research performed with porous particles is very limited (Bindgen et al., 2022; Bossler & Koos, 2016), and has focused only on the influence of variations in the contact angle, while the amount of secondary liquid was kept constant (Bossler & Koos, 2016). Knowledge on how water absorption influences the distribution of water and subsequent bridge formation for varying amounts of water is still missing. Also the influence of surface roughness on capillary suspension rheology is, to the best of our knowledge, limited to only one study (Allard et al., 2022). Surface roughness influences rheological behavior through effects on the contact angle between bridges and particles. As the relationship between roughness and the contact angle is difficult to predict (Ballard, Law, & Bon, 2019), results obtained for one particle type cannot be directly transferred to other particle types. In addition, for synthetic particles, effects of particle properties have been mostly investigated separately, while for biopolymeric particles, the effect of water absorption is always intertwined with that of variation in other particle properties.

Therefore, in this study, we aim to gain insights into the effect of different particle properties for biopolymeric particles. We utilize protein particles, which can be used for both food and pharmaceutical applications. We vary particle size and water absorption capacity (WAC) – the latter by changing the internal structure of the particles, which also affects their surface structure – and observe the effects of these particle properties on gel strength and network structure. Such knowledge adds to our general understanding on how water absorption and particle swelling influence the formation of capillary suspensions. In addition, protein-based capillary suspensions, also known as protein oleogels, are currently of high interest for solid fat replacement in a variety of food applications (de Vries et al., 2018; Manzoor, Masoodi, Naqash, & Rashid, 2022; Wang et al., 2022), but more knowledge on how the texture properties of these oleogels can be adjusted over a broad range is necessary. We hypothesize that variation in size and WAC has a large influence on the formation of the particle network and the properties of the final systems.

To systematically vary protein particle properties, we employ an emulsion-based approach to obtain spherical protein particles with controlled WAC and size by adjusting pH and emulsification conditions. These particles are then introduced into oil as a primary liquid to obtain oleogels, and water is added as the secondary bridging liquid. The macroscopic appearance of the gels, the location of the water within the system, and the gel strength are discussed, and then related to the network structure as evaluated by microscopy and neutron scattering.

2. Materials and methods

2.1. Sample preparation

2.1.1. Preparation of protein particles

Protein particles were prepared as described by Sağlam, Venema, de Vries, Sagis, and van der Linden (2011) with some modifications. A 25 wt% whey protein isolate (WPI)-solution (BIPRO 9500, Agropur, Le Sueur, MN, U.S.) and a 4 wt% sodium caseinate (NaCas)-solution (Ecellion EM7, FrieslandCampina, Veghel, the Netherlands) were prepared by dissolving the protein powders under continuous stirring for 2 h at room temperature in demineralized water. Before usage, the protein solutions were stored overnight at 4 °C to allow complete protein hydration. For preparation of protein particles with high water absorption capacity (WAC), the pH of the WPI-solution was left unadjusted (approx. pH 6.8), whereas for the preparation of protein particles with a low WAC it was adjusted to a pH of 6.2 by addition of 1 M and 0.5 M HCl-solution. Following the initial pH-adjustment, the pH-value was remeasured after 30 min, and if necessary readjusted. Polyglycerol polyricinoleate (PGPR, Grindsted PGPR 90, Danisco, Grindsted, Denmark) was dissolved in sunflower oil (Reddy sunflower oil, Vandemoortele Nederland BV, Zeewolde, the Netherlands) by stirring for 2 h at room temperature at concentrations of either 0.25% or 1%, to prepare large and small protein particles, respectively.

Water-in-oil emulsions were then obtained by dispersing the previously prepared WPI-solutions in sunflower oil containing PGPR in a ratio of 1:9 (w/w) with a rotor–stator homogenizer for 5 min at 13 000 rpm (T25 digital Ultra Turrax, IKA-Werke, Staufen, Germany). The obtained emulsions were then immediately heated in a water bath at 80 °C for 20 min to induce protein gelation. This heating step was performed under gentle stirring to prevent agglomeration of the forming protein particles. Subsequently, the obtained dispersions containing the protein particles were cooled down in an ice bath, and centrifuged at 20 °C and 10 000 g for 60 min. The pellet was first redispersed in the NaCas-solution in an approximate ratio of 1:2 (v/v) using a rotor–stator homogenizer (at a speed appropriate to obtain a homogeneous dispersion). The obtained dilute dispersion was then sonicated for further break up of particle agglomerates formed during the heating step.

Sonication was performed at an amplitude of 70% for 5 min in pulse mode (0.5 s on, 0.5 s off), to prevent overheating of the samples (Branson Digital Sonifier 450, BRANSON Ultrasonics Corporation, Danbury, CT, U.S.). The sonicated dispersions were centrifuged again with the same settings to collect the protein particles, and the washing step with the NaCas-solution was repeated for a second time. In this second washing step, sonication was performed only if reagglomeration during the centrifugation step had occurred, which was determined by monitoring changes in particle size distribution (PSD) as described below. The final pellet obtained from this second washing step was the starting point to prepare the protein oleogels.

2.1.2. Transfer of protein particles to oil

The obtained protein particles were transferred to oil based on a solvent transfer method as has been previously described by de Vries, Wesseling, van der Linden, and Scholten (2017). The aqueous protein pellet was redispersed in analytical-grade acetone with a rotor–stator homogenizer (T25 digital Ultra Turrax, IKA-Werke, Staufen, Germany) in an approximate ratio of 1:10 (v/v), and the obtained dispersion was centrifuged at 20 °C and 10 000 g for 20 min. The pellet was subsequently washed once more with acetone, and then twice with sunflower oil, following the same procedure. During the two washing steps with oil, any large visible grains present in the protein pellets were discarded. The remaining oil-based pellet was redispersed for a final time in oil and left under stirring overnight at room temperature to allow remaining acetone to evaporate, which has been shown to lead to practically acetone-free samples (de Vries et al., 2017). After a last centrifugation step, again at 20 °C and 10 000 g for 20 min, the final protein oleogel was obtained. Before using these gels for further analysis, they were homogenized with a rotor–stator-homogenizer to ensure a homogeneous structure. To obtain sufficient material for all measurements, two separate batches were prepared per particle type, and then combined. To verify that these separately prepared batches had indeed similar properties, the protein content and PSDs were determined individually per batch.

2.1.3. Protein content determination

The protein content of the oleogels was determined externally by bilacon GmbH (Berlin, Germany), using the Dumas method (FP828 nitrogen analyzer, LECO Europe B.V., Geleen, the Netherlands) with helium as carrier gas. Measurements were done in triplicate for each separately prepared batch per oleogel type, and the protein content was calculated from the determined nitrogen content, N, using a protein-specific conversion factor of 6.38 (Maubois & Lorient, 2016) (protein content = $N \times 6.38$).

2.1.4. Water content determination

The water content of the oleogels was determined gravimetrically by water evaporation in an oven at 105 °C for 4 h (Venticell, BMT Medical Technology, Brno, Czech Republic). Approximately 1 g of sample was added to aluminum cups, which were preheated to prevent possible water contamination from the cups. The approximate water content was then determined in duplicate from the change in sample weight before and after drying.

2.1.5. Creating capillary suspensions by water addition

To obtain capillary suspensions, the protein content of the previously prepared oleogels was first standardized by the addition of sunflower oil and manual mixing with a spatula. Then, the desired amount of demineralized water was added slowly within 2 min while mixing with a rotor–stator homogenizer at 13 600 rpm (T25 digital Ultra Turrax, IKA-Werke, Staufen, Germany). As this homogenization method was already applied during preparation and transfer of the particles to oil, we do not expect any effect of this step on the particle properties. Mixing was continued for another 3 min to distribute the water homogeneously. Then, the oleogels were degassed for 10 min with a vacuum pump to remove enclosed air bubbles. In case air bubbles were still present, the samples were vortexed, and degassed again for 10 min. Before using the samples for further analysis, they were stored at 4 °C overnight, to allow diffusion processes of the added water to finish. In the following, the amount of added water is expressed as g water/g protein.

2.2. Sample characterization

2.2.1. Particle size distribution

The particle size distribution (PSD) of the protein particles in water and oil was determined by static light scattering (Malvern Mastersizer 3000 with a Hydro MV dispersion unit, Malvern Instruments Ltd, Worcestershire, UK), based on Mie theory. Values for refractive indices were set to 1.33 for water, 1.47 for sunflower oil, and 1.45 and 1.54 for protein in water or oil, respectively. PSDs of the protein particles in water were determined during both washing steps with NaCas-solution, after redispersion of the protein particles by homogenizing with a rotor–stator homogenizer (T25 digital Ultra Turrax, IKA-Werke, Staufen, Germany) and after sonication. PSDs in oil were recorded from the final oleogels by dispersing a small amount of oleogel in sunflower oil with a rotor–stator-homogenizer. Measurements were done in triplicate for each of the two batches prepared per particle type, and obtained PSDs are reported as volume-based distributions.

2.2.2. Determination of difference in water absorption capacity (WAC)

To confirm the expected difference in water absorption capacity (WAC) for protein particles prepared at different pH-values, macroscopic gels were prepared in syringes (diameter 2 cm) at two pH-values (unadjusted at approx. pH 6.8 and pH 6.2). Here we took care to keep the WPI-concentration (25%) and heating time and temperature (20 min at 80 °C) the same as for the original preparation of the micron-sized protein particles. The gels were sliced into cylinders (height 1.5 cm) with a gel cutter, and immersed into demineralized water for 30 min. Afterwards, the gel slices were placed on a metal grid to allow excess water to drip off, and then carefully blotted dry with a tissue. The weight difference before and after water immersion was recorded to determine the amount of water absorbed by the gel. For both pH-values, two macroscopic gels were prepared separately, and per gel three slices for WAC-determination were obtained.

2.2.3. Oscillatory rheology

To quantify the gel strength (storage modulus, G') of the oleogels, oscillatory rheology was performed with sandblasted, parallel plates (upper plate model PP50/S, lower plate Inset I-PP50/SS/S, diameter 50 mm) on a shear-controlled MCR 502 rheometer (Anton Paar GmbH, Graz, Austria). Samples were left to equilibrate during a 15 min preshear period at a frequency of 1 Hz and an amplitude of 0.01%. Subsequently, an amplitude sweep was performed by increasing the amplitude to 1000% in 520 s at constant frequency of 1 Hz. Using the instrument software, the gel strength was determined as the value of the storage modulus G' at the end of the linear viscoelastic regime, which was defined as the G'-value at which the G'-curve has decreased by 5% from its average plateau value. Measurements were performed in duplicate for each sample.

2.2.4. Confocal Laser Scanning Microscopy (CLSM)

Particles were imaged in water and oil with a Re-Scanning Confocal Microscope (RCM1, confocal.nl, Amsterdam, the Netherlands). To image protein particles in water, the dispersion of particles in NaCas-solution obtained during the first washing step was diluted with demineralized water in an approximate ratio of 1:20 (v/v), and stained with a drop of 0.2 wt% Rhodamine B dissolved in demineralized water. Images of protein particles in water were taken before and after sonication at an excitation wavelength of 561 nm. Protein oleogels were imaged undiluted. They were stained by adding 0.2 wt% Rhodamine

B dissolved in ethanol in a concentration of 6 μL/g oleogel. The dye solution was mixed with the oleogel by stirring with a spatula, and stained samples were stored protected from light in the fridge until imaging at an excitation wavelength of 561 nm. Per oleogel type and added amount of water, around 20 images were taken at constant laser power and imaging depth. The imaging depth for each sample was chosen individually, so that the collected signal was sufficient for structures to still appear clearly, but at a depth large enough for the sample structure to be unaffected by the cover glass (as observed by the sample structure remaining unchanged when increasing the imaging depth). Additionally, water bridges were imaged in a qualitative fashion after adding a 3% Nile Blue-in-oil-solution in a ratio of 1:1 (v/w). As the size of the water bridges is close to the resolution limit of the microscope, for this purpose an oleogel from larger particles was prepared (0.2 wt% PGPR, high WAC, $d_{4,3}$ = 20 μm). Oil and protein were distinguished by the use of different excitation wavelengths; 640 nm for protein, and 488 nm for oil.

2.2.5. Post-processing of CLSM images for quantitative image analysis

The CLSM images of the protein oleogels from large particles with high WAC were post-processed using the supervised machine learning toolkit for automated image analysis Ilastik (Berg et al., 2019), followed by a custom analysis code in MATLAB (version r2023a, MathWorks). For each water content, a minimum of 17 CLSM images were analyzed, ensuring that these images capture a wide range of particle arrangements. The analysis algorithm was trained using a selection of three representative images. To obtain binary segmentation, parts of the image indicative of protein particle and oil phase areas were manually marked. This initial training was performed until individual particles could be accurately distinguished. To refine the detection of particles, a core threshold value of 90% and a rim threshold of 50% were applied, and particles of a size below 0.01 μm^2 were discarded. Subsequently, batch processing was utilized for all images. For an exemplary illustration of the image processing steps in Ilastik, see **Supplementary Material S1**. Based on the particle positions and area identified by Ilastik, the number of nearest neighbors, N, minimum neighboring distance, D, and Hopkins statistic index, H (Banerjee & Dave, 2004; Jain & Dubes, 1988), were then calculated using a custom-made code in MATLAB.

2.2.6. Scanning electron microscopy (SEM)

Dilute dispersions of large protein particles with high and low WAC and large silica particles in oil were added to a poly-L-lysine glass plate. 2.5% glutaraldehyde in 0.1 M phosphate/citrate buffer was then added for a first fixation step and incubated for a minimum of 60 min at room temperature. Subsequently, this first fixative was removed by washing with 0.1 M phosphate/citrate buffer six times for 10 min. As a second fixation step, 1% osmium tetroxide in 0.1 M phosphate/citrate buffer was added and incubated for approximately 60 min at room temperature, after which this second fixative was removed by washing three times with MilliQ-water for 10 min. Subsequently, the protein samples were dehydrated in 8 steps using an increasing ethanol percentage (30%, 50%, 70%, 80%, 90%, 96%, twice 100%), dried in a critical point dryer (Leica EM CPD300, Leica Microsystems B.V., Amsterdam, the Netherlands) in 100 % ethanol, and attached to aluminum stubs. Lastly, the samples were coated with 12 nm tungsten and observed using a scanning electron microscope (FEI Magellan 400, Thermo Fisher Scientific, Eindhoven, the Netherlands) with an acceleration voltage of 2 kV.

2.2.7. Cryo-scanning electron microscopy (cryo-SEM)

The distribution of water between the protein particles was imaged by cryo-SEM, for which a small amount of oleogel with added water was placed on a cryo-sample holder and rapidly frozen in liquid ethane. After further cooling with liquid nitrogen, samples were transferred under vacuum to a cryo-preparation system (MED 020/ VCT 100, Leica, Vienna, Austria). Following cryo-fracturing at approximately −90 °C, a freeze-drying step was applied for 3 min to etch and remove any water vapor contamination. Subsequently, samples were cryo-shielded and analyzed with a field emission scanning microscope (FEI Magellan 400, FEI Company/Thermofisher, Hillsboro, OR, U.S./Waltham, MS, U.S.) equipped with a Leica cold stage for cryo-SEM at a working distance of approximately 4 mm, with secondary electron detection at an acceleration voltage of 2 kV.

2.2.8. Spin-echo small-angle neutron scattering (SESANS)

Spin-echo small-angle neutron scattering (SESANS) measurements, suitable to investigate structures on length scales from 30 nm to 20 μm (Bouwman, 2021), were performed on the SESANS instrument at the Delft University of Technology. For further technical details we refer to Rekveldt et al. (2005). To increase scattering contrast, D_2O was added to H_2O in a D_2O:H_2O ratio (w/w) of 1.53:1. To keep the volume fraction of secondary liquid constant, the amount of added H_2O-D_2O-mixture was chosen to match the amount of H_2O added to oleogel samples prepared for rheology and imaging by volume rather than by weight. While all samples with added H_2O-D_2O-mixture were measured at a sample thickness of 1 mm, the sample without added water was measured with a thickness of 4 mm to obtain sufficient scattering. Measurements were performed in duplicate on two separately loaded samples. For gels without added water, an additional duplicate measurement on a slightly diluted oleogel at a protein concentration of 18.5% was performed.

Using the software SasView 5.0.5 (Bakker et al., 2020; Sasview, 2022), the scattering length density of protein particles and fractal dimension were estimated by fitting the obtained normalized scattering correlation function to the Hankel transform of the fractal model (NIST IGOR/DANSE, 2017; Teixeira, 1988):

$$I(q) = \phi V_p(\rho_p - \rho_o)^2 P(q) S(q) + \text{background} \tag{2}$$

where ϕ is the volume fraction of the protein particles with radius R_0, V_p is the volume of a protein particle ($V_p = \frac{4}{3}\pi R_0^3$), ρ_p and ρ_o are the scattering length densities of the protein particles and sunflower oil, respectively, and *background* specifies the source background. $P(q)$ is defined as

$$P(q) = F(qR_0)^2 \tag{3}$$

for which $F(q)$ is given as

$$F(qR_0) = \frac{3(\sin(qR_0) - (qR_0)\cos(qR_0))}{(qR_0)^3} \tag{4}$$

$S(q)$ is defined as

$$S(q) = 1 + \frac{D_f \Gamma(D_f - 1)}{\left[1 + \frac{1}{(q\xi)^2}\right]^{(D_f-1)/2}} \frac{\sin\left[(D_f - 1)\tan^{-1}(q\xi)\right]}{(qR_0)^{D_f}} \tag{5}$$

where ξ represents the cluster size (correlation length) and D_f the fractal dimension.

Values of ρ_o, ϕ and ξ were provided as input parameters for the fractal model, from which ρ_p and D_f were obtained as fitting parameters from the best fit through the experimental data points. The value of ρ_o was set to 0.225×10^{-6} Å^{-2} and ξ to 40 μm. For the particle volume fraction ϕ, the sum of the volume fraction of protein particles and added water was provided. The volume fraction of protein particles was calculated based on a protein particle density of 1.2×10^3 kg m^{-3}, which was estimated based on a density of protein of 1.43×10^3 kg m^{-3} (Quillin & Matthews, 2000) and assuming that particles absorb 50% sunflower oil of a density of approximately 0.9×10^3 kg m^{-3}. The value of R_0 was determined to be 0.7 μm by fitting the obtained scattering data for the sample without added water to a sphere-model (Guinier, Fournet, Walker, & Yudowitch, 1955; NIST IGOR/DANSE, 2014) by using Eq. (2) with $S(q) = 1$. This value was used for all samples with varying amounts of added water. For a more detailed discussion see **Supplementary Material S2.**

For interpretation of results, for water, deuterium and pure protein, scattering length densities ρ of -0.56×10^{-6} Å^{-2}, 6.48×10^{-6} Å^{-2} and 2.00×10^{-6} Å^{-2} were taken, respectively.

3. Results and discussion

3.1. Preparation of spherical protein particles varying in water absorption capacity and size

Via an emulsion-based method (see Section 2.1.1), three different types of spherical protein particles varying in size and water absorption capacity (WAC) were obtained: Small particles with high WAC, large particles with high WAC, and large particles with low WAC. The size varied between a diameter of around 1 μm for small and 10 μm for large particles. WAC was varied via variations in the internal network structure of the particles, achieved by gelling the emulsion droplets at different pH-values. At lower pH-values, i.e. at pH-values closer to the isoelectric point of the whey protein isolate at a pH of approximately 5 (Lam & Nickerson, 2015), a denser, more particulate structure is obtained (Nicolai & Durand, 2013). Particles with such denser networks are expected to have a lower WAC than more fine-stranded particles. The variation in WAC was quantified by preparation of macroscopic aqueous gels (25 wt% protein), obtained at the same pH-values and heating conditions as applied for particle preparation. Assuming that the WAC is similar for micron-sized particles and macroscopically large gels, we gravimetrically determined the amount of absorbed water. Gels prepared at pH 6.2 absorbed 0.038 ± 0.004 g water/g gel and gels prepared at 6.8 absorbed 0.100 ± 0.004 g water/g gel. The WAC of these macroscopic, aqueous gels therefore varied by a factor of 2.5, with gels prepared at higher pH indeed having a higher WAC.

Overall, we were able to prepare spherical protein particles varying in WAC and size, allowing us to gain more insights into the effect of different particle properties on capillary bridge formation. For a more detailed discussion of the particle preparation procedure and particle properties, see **Supplementary Material S3**. In **Supplementary Material S4**, also the water and protein content of the oleogels as obtained from centrifugation of the final protein particle dispersions in oil is provided and discussed.

3.2. Distribution of water

After standardization of the protein content of the oleogels prepared from the three different protein particle types (20% for high WAC-oleogels, 19% for low WAC-oleogels), water was added to the gels in an amount of up to 2.8 g/g protein, to induce the formation of capillary bridges. The macroscopic appearance of the obtained oleogels (Fig. 1) indicates that addition of water led to a significant change in the gel properties, especially for oleogels prepared from large particles. For these particles, the gels without added water appear as flowable liquids, around 0.8 g/g as semi-solid gels, and at the highest amounts of added water, the gels appear as grainy, coarse materials. An increase in firmness is also visible for the oleogels prepared from small particles; however, the change in appearance is less drastic. Moreover, the oleogel was already visually becoming weaker at 1 g/g of added water. Therefore, the range of added water was not extended further in case of the small particles. These results already show the importance of the particle properties, particularly their size.

Apart from changes in gel strength, the gels also became transparent at a water content of around 0.8 g/g to 1 g/g, after which they became more opaque again. This effect can be attributed to a change in the refractive index of the protein particles, due to absorption of water (de Vries et al., 2018). The refractive index (RI) of pure protein is 1.6 (McMeekin, Groves, & Hipp, 1964); with the increasing absorption of water in the particles (RI = 1.33), the RI decreases until it becomes similar to that of sunflower oil (RI = 1.47). Upon further water absorption, the refractive index of the protein particles decreases to values lower than that of the oil, leading again to an opaque appearance. As the protein content of the different particles was the same, the similar amount of added water leading to maximum transparency indicates that the amount of absorbed water was similar for different particle types. However, visual observation of samples is an approximate fashion to determine changes in RI, and the RI may also be influenced by the difference in network structure for low and high WAC-particles and related differences in water distribution throughout the particles.

To obtain further insights into the water distribution within the systems, we analyzed the samples using spin-echo small-angle neutron scattering (SESANS). This method was only suitable for oleogels prepared from small particles, as the size of the large particles utilized in this research was above the maximum length scale of the SESANS-technique. Fig. 2a shows the obtained scattering data presented as the normalized scattering correlation function $G(\delta)$, taking into account measurement-specific parameters as the neutron wavelength and sample thickness, with δ being the spin-echo length and $G(0)$ being the signal strength (Bouwman, 2021). As data obtained from two separately performed duplicate measurements was consistent, here results are shown for only one of the two measurements performed per sample. To increase contrast, deuterated water instead of normal water was added to the oleogels. As expected, the scattering intensity, $G(\delta) - G(0)$, increased (became more negative) with an increasing amount of added H_2O-D_2O-mixture. The continuous, gradual decrease of the curves indicates the presence of a network rather than of separate particles (Bouwman, 2021). Thus, a fractal model (Section 2.2.8) was chosen to fit the data, from which values for the scattering length density of the protein particles, ρ_p, and for the fractal dimension could be obtained. As the scattering length density is related to the scattering ability of the material, it provides information on the material properties, which are influenced by the presence of water. Therefore, changes in ρ_p can provide information about the occurrence of water absorption. Results for the fractal dimension are relevant to network structure and are discussed in Section 3.4.

To fit the obtained scattering data to the fractal model, the radius of the protein particles was provided as an input parameter. This particle radius was obtained by fitting the scattering data of oleogels without added water to a sphere-model and determined as 0.7 μm; for details see the methods Section 2.2.8 and **Supplementary Material S2**. Using this value for the particle radius R_0, values for ρ_p from fitting of the scattering data to the fractal model were obtained and are shown as function of water addition in Fig. 2b. Before the addition of water, ρ_p was around 0.7×10^{-6} Å^{-2}, which is much lower than the scattering length density of pure protein of around 2.0×10^{-6} Å^{-2}. This indicates that the protein particles had a considerable amount of oil ($\rho_o = 0.225 \times 10^{-6}$ Å^{-2}) absorbed, which is expected due to the protein particles' porous nature (Plazzotta, Calligaris, & Manzocco, 2020). Then, with increasing amounts of added water (H_2O-D_2O-mixture, $\rho_w = 3.52 \times 10^{-6}$ Å^{-2}), ρ_p increased, meaning that in line with observed changes in refractive index of the macroscopic gels (Fig. 1), water was absorbed by the protein particles. At higher amounts of added water, ρ_p begins to plateau, which indicates that the particles were approaching a state of maximum absorption.

Such changes in scattering length density can be used for the quantitative determination of the proportion of water absorbed by the particles compared to the amount of water remaining between them. First, in Eq. (6), we define the different components of the gel as the gel's particle volume fraction, $\phi_p^{(0)}$, which denotes the particles consisting of protein and oil as present in the gel before water addition, the oil phase in which the particles are dispersed, ϕ_o, and the added H_2O-D_2O-mixture, ϕ_w:

$$\phi_p^{(0)} + \phi_o + \phi_w = 1 \tag{6}$$

For these volume fractions, $\phi_p^{(0)}$ and ϕ_o can be obtained from the known weight-based protein content of the gels (for details, see Section 2.1.3) by estimating the density of the particles (i.e. the particles consisting of protein and oil, in absence of added water). As described in Section 2.2.8, we assumed that particles absorb 50% sunflower oil

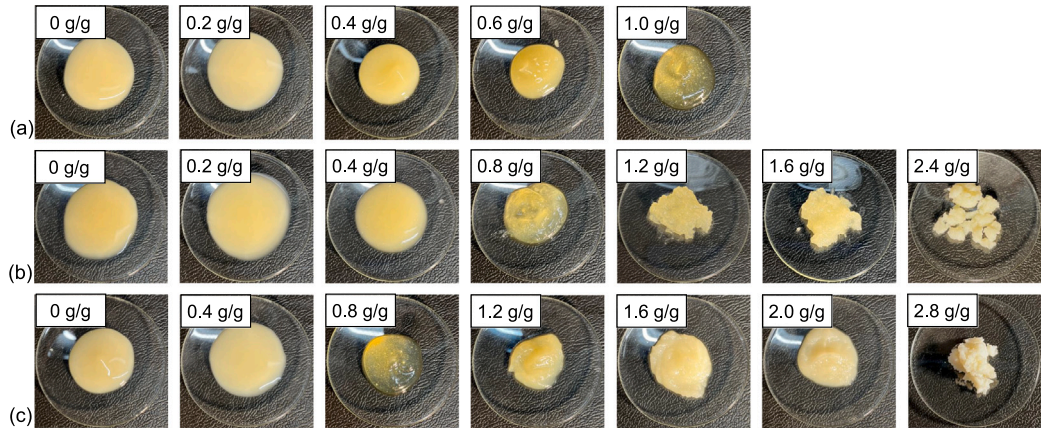

Fig. 1. Appearance of protein oleogels at increasing amount of added water for gels prepared from particles with (a) small size and high WAC, (b) large size and high WAC and (c) large size and low WAC.

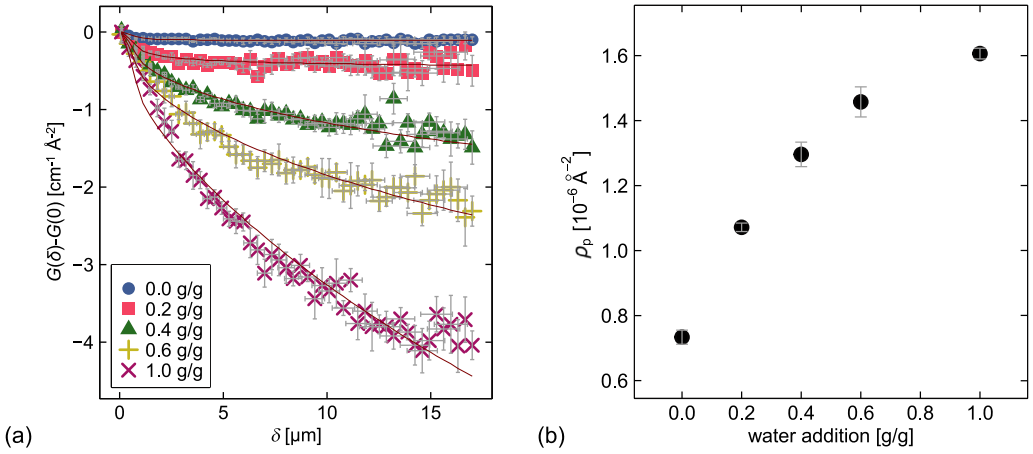

Fig. 2. (a) SESANS-signal obtained for oleogels prepared from small particles at increasing amount of added water. The fits to the applied fractal model are indicated by red lines. Results are shown for one of the two consistent measurements per sample, which were each performed in duplicate. (b) Scattering length density, ρ_p, of protein particles from oleogels prepared with small particles obtained from SESANS-signal fits shown in (a) as average value from the two performed measurements.

of a density of approximately $0.9 \times 10^3\,\mathrm{kg\,m^{-3}}$. Taking a density of protein of $1.43 \times 10^3\,\mathrm{kg\,m^{-3}}$ (Quillin & Matthews, 2000), a density of $1.2{\times}10^3\,\mathrm{kg\,m^{-3}}$ is obtained for the particles. The amount of water added to the gels, and thus its volume fraction, ϕ_w, is known.

For the scattering length densities of the different components, the scattering length densities of oil and water, ρ_o and ρ_w, are known values. From fitting of the scattering data for the gel without added water, also the scattering length density of the particles without absorbed water, $\rho_p^{(0)}$, is known. From this, the fraction of water absorbed in the particles, ϕ_w^p, and thus the quantitative distribution of water in the gels, can be calculated from ρ_p obtained for gels with varying amounts of added water (Fig. 2b) according to Eq. (7) as

$$\rho_p = \frac{\phi_p^{(0)} \cdot \rho_p^{(0)} + \phi_w^p \cdot \rho_w}{\phi_p^{(0)} + \phi_w^p} \tag{7}$$

from which we can isolate the volume fraction of water absorbed in the particles, ϕ_w^p, as shown in Eq. (8) as

$$\phi_w^p = \frac{\phi_p^{(0)} \cdot \rho_p^{(0)} - \phi_p^{(0)} \cdot \rho_p}{\rho_p - \rho_w} \tag{8}$$

To calculate ϕ_w^p from Eq. (8), the particle volume fraction for the gels without added water, $\phi_p^{(0)}$, serves as a direct input value. As described above, this requires an estimation of the amount of oil present in the particles, as already before water is added the protein particles do not only consist of protein, but have some oil absorbed. In addition, the particle volume fraction of the gels is needed as input parameter for fitting to the fractal model (Eq. (2)) to obtain the scattering length density of the particles, ρ_p. Thus, to obtain correct values for ρ_p, an accurate estimation of the particle volume fraction is crucial. For the gels with added water, not only the amount of initially absorbed oil, but also the change in particle volume fraction due to water absorption needs to be taken into account. The amount of water absorbed depends on how the water distributes within and between particles, which is actually unknown and is the reason to perform these experiments. Moreover, water absorption can cause the particles to release oil, making an accurate estimation of the protein volume fraction difficult.

Oil release from the particles (defined as protein with initially absorbed oil) does not only influence the particle volume fraction, but also their scattering length density. This scattering length density of the particles without absorbed water, $\rho_p^{(0)}$, is used to calculate the water distribution according to Eq. (8). As this value depends on the specific protein–oil ratio, it is influenced by oil release upon water absorption. Therefore, calculating the water distribution using the value of $\rho_p^{(0)}$ obtained for the gels without added water does not yield accurate results for gels with added water. For accurate information on the composition in terms of protein–oil ratio and thus scattering length density of the particles, the relation between water uptake and oil release also needs to be known. In a study on water absorption and accompanying oil release in millimeter-sized protein microgel particles (unpublished), it was shown that in relation to their total weight,

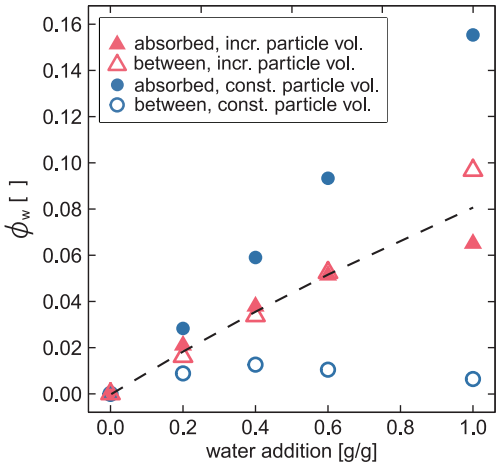

Fig. 3. Water fraction of the gels that is either absorbed by the protein particles or remains in between them as determined from SESANS-measurements. The amount of water located between the particles was calculated by subtracting the fraction of absorbed water, ϕ_w^p, obtained from Eq. (8), from the known total water fraction of the gels, ϕ_w. Results for the two extreme situations of an increase of the particle volume fraction by the full amount of added water (scenario 1) or a constant particle volume fraction (scenario 2) are shown. The dashed line represents equal partitioning of the added water, i.e. a distribution of half of the water being absorbed, and half remaining between the particles.

around 10% of oil was released from the particles when immersed in water. As this leads to a rather small change in $\rho_p^{(0)}$ only, the influence of oil release on the particles' scattering length density will be much less relevant than the effect of changes in the estimated particle volume fraction due to water absorption and oil release, but is nonetheless an additional factor to take into account.

A correct estimation of the particle volume fraction to obtain accurate results for the water distribution ultimately depends on precise knowledge on the water distribution, making the proposed calculation a circular problem. To gain first insights, we can determine an upper and lower boundary for both the amount of absorbed water and water located between the particles by assuming two most extreme, theoretical scenarios for the volume fraction; (1) the volume fraction increases by the full amount of added water, or (2) the change in the volume fraction of particles upon water addition is negligible. In the first scenario, all water would be absorbed by the particles, and no oil would be released. The second scenario approximates both the situation where only a very small amount of water is absorbed by the particles and the situation where an equivalent volume of oil is released once water is absorbed – but we neglect changes in $\rho_p^{(0)}$ due to oil displacement in the latter situation. The obtained water distributions calculated for these two extreme situations are provided in Fig. 3.

Assuming that the particle volume fraction increases by the amount of added water (scenario 1, red triangles), the water would be distributed in approximately equal amounts (50%) within and between particles up to 0.6 g/g of added water. For higher water contents, the amount of water absorbed by the particles begins to plateau (closed red triangles), while the amount of water between the particles (open red triangles) keeps increasing. Thus, in this scenario, at larger amounts of added water, more water is located between the particles than within (up to ~ 60%). Assuming a constant particle volume fraction (scenario 2, blue circles), already from the lowest amount of added water, the amount absorbed in the particles (closed blue circles) is larger than the amount in between particles (open blue circles). With increasing amounts of added water, the amount of absorbed water increases linearly, while the amount of water between the particles plateaus first, and then even decreases. Thus, in this scenario, the amount of water absorbed within particles (~ 75-95%) is much larger than that located between particles (~ 25-5%) at all amounts of added water. However, the results of this second scenario seem unrealistic. As the particles have a maximum water absorption capacity, water uptake is expected to be limited at a higher water content. In the high water addition regime, further addition of water should therefore lead to a more reduced increase of absorbed water, resulting in a larger fraction of water present between the particles, as obtained for the first scenario. Scenario 1 is therefore much more realistic.

While at low amounts of added water results for the two scenarios are more similar, they start to strongly deviate for larger amounts of added water. According to scenario 1, around 40% of the added water would be absorbed, whereas it would be almost all water for scenario 2. Clearly, estimation of the correct particle volume fraction is of great importance for determination of the water distribution. Although precise determination is difficult, the obtained results provide a first range for the amount of water absorbed or located between the particles, and shows that water absorption and bridge formation do not occur sequentially, but simultaneously; water is present between particles at all measured water contents. In addition, the WAC of the particles was determined as > 3 g water/g protein (see Section 3.1, taking into account that the macroscopic gels used for determination of WAC upon immersion in water already consisted by 75% of water). Water was already located between the particles at much lower amounts of added water. Next to that, according to scenario 1, the amount of absorbed water had already begun to plateau at 1 g/g (Fig. 3), i.e. at an amount of added water much below the maximum absorption capacity of the particles. This would indicate that arrangement of the added water between the particles in form of water bridges is energetically not unfavorable compared to absorption of water.

Although water bridges are expected to be present based on the SESANS results (Fig. 3) and the changes in macroscopic appearance of the gels (Fig. 1), it is difficult to visualize those bridges for protein particles. This can be attributed to the small size of protein particles and bridges, and difficulties in signal separation due to the location of the bridging liquid not only between, but also within the particles. By working with well-defined, spherical protein particles of much larger size, we were able to visualize – to our knowledge for the first time – water bridges between protein particles as shown in Fig. 4. For a more detailed discussion of these images and for the results of an attempt to image the water bridges also by cryo-SEM, we refer to **Supplementary Material S5**.

By applying a combination of different techniques, we demonstrated that the added water in case of capillary suspensions prepared from highly absorbing, biopolymeric particles is indeed partly absorbed by the particles, and partly located in between them. The SESANS results show that such distribution is already present at the lowest amounts of added water, meaning that water absorption and bridge formation occur simultaneously rather than consecutively.

3.3. Gel strength

To quantify variations in gel strength that result from differences in particle properties (size and WAC), we employed oscillatory shear rheology to oleogels prepared from various particle types before the addition of water, and upon capillary bridge formation, i.e. upon addition of increasing amounts of water. The storage modulus, G', and its relative change compared to the sample with no added water, G'/G'_0, are shown in Fig. 5.

When we compare G' for small and large particles at high WAC without added water, G' of the oleogel prepared from small particles was higher by approximately one decade. This can be attributed to the higher total surface area for small particles, and therefore a higher degree of interactions between particles. These results are in line with previous research on oleogels prepared with protein (Feichtinger et al., 2022) or silica particles (Koos et al., 2012). Interestingly, we see that oleogels from particles with low WAC show a significantly higher G', even exceeding G'-values of oleogels from smaller particles. As no

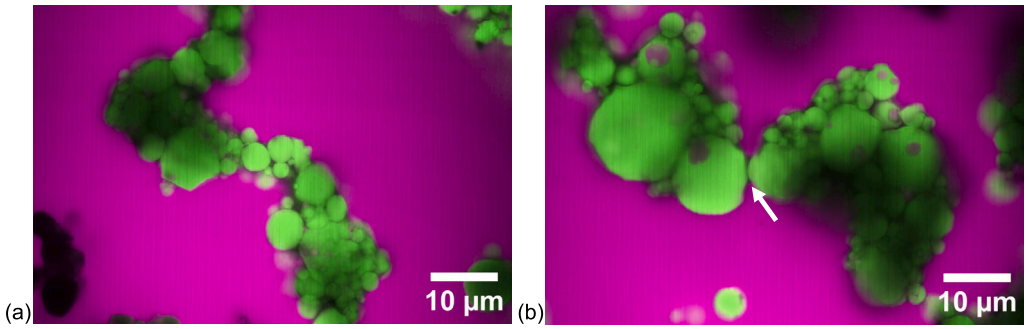

Fig. 4. CLSM images of protein oleogels with protein particles of an average size of 20 µm ($d_{4,3}$), high WAC, stained with Nile Blue to distinguish between protein (green), oil (magenta) and water (black). Amount of added water 2.0 g/g protein. In (b), the white arrow points to a liquid bridge between two particles.

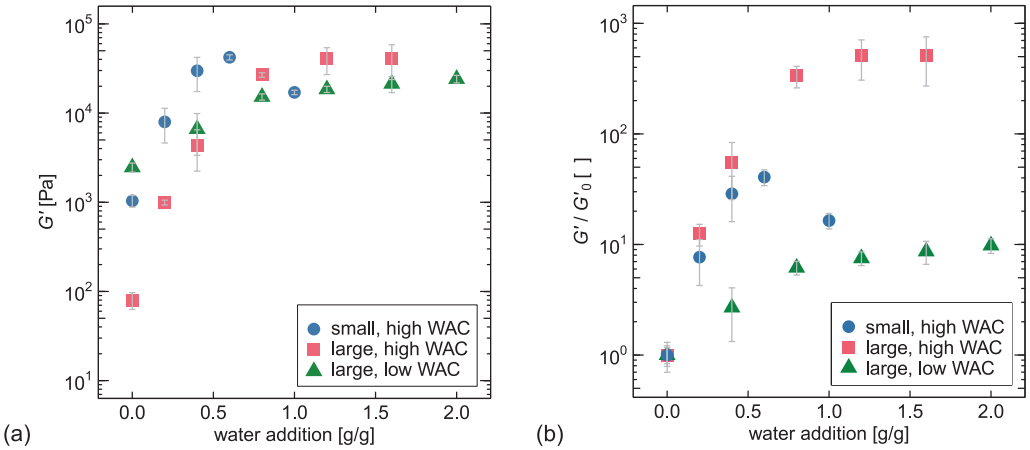

Fig. 5. Gel strength, G', of oleogels prepared from different particle types upon addition of an increasing amount of water, (a) in absolute values with error bars indicating standard deviations of duplicate measurements and (b) normalized by the G'-value of the oleogel before water addition (G'_0).

water was added to the oleogels, the difference in gel strength cannot be caused by differences in water absorption, but must be due to the properties of the particles themselves. For WPI-microgel particles as prepared in this study, it has already been shown that a variation in the internal network structure by variation of the pH-value during denaturation does not only influence the WAC, but also the particles' surface structure. Particles prepared at lower pH-values with a denser network structure also show a rougher surface structure (Sağlam, Venema, de Vries, van Aelst, & van der Linden, 2012). A higher surface roughness for the low WAC particles is also supported by SEM images of the particles prepared in the current study, see **Supplementary Material, Figure S3.3d**. Such higher surface roughness for low WAC particles provides increased interparticle contact and particle interlocking (Müller, Isa, & Vermant, 2023; Wilson & Davis, 2000), which has been shown to increase suspension viscosity (Zhang, Arrighi, Campbell, Lonchamp, & Euston, 2016). This is in line with Fig. 5a: The higher G' for low WAC-particles indicates that for large particles varying in WAC, not only differences in WAC, but also subsequent variations in surface roughness were important.

Upon addition of water, G' first increased considerably for all oleogel types, and then either reached a plateau (large particles) or decreased again (small particles). These results are in line with earlier results from literature (de Vries et al., 2018; Domenech & Velankar, 2017; Koos, 2014; Li et al., 2023). As protein particles are of hydrophilic nature, we assume that the contact angle between particles and water was below 90°, and capillary systems in a pendular state are thus expected (Bossler & Koos, 2016). The formation of such pendular bridges with a concave shape was indeed confirmed in CLSM images, as discussed in the **Supplementary Material S5** and shown in Fig. 4. Therefore, when water was added, the formation of pendular capillary bridges first led to increased attractive interactions between particles and an increase in G', until a state of full bridging was reached. Then, further addition of water merely led to an increase of the volume of the liquid bridges, and no changes in G' occurred. When the bridge volume increased to an extent that neighboring bridges merged, a state of full bridge formation was reached, and particles first started to agglomerate in trimers, referred to as funicular state. When more water was added, large compact particle clusters formed, and the gels became weaker, as has been discussed in literature (Bossler & Koos, 2016; Dittmann & Willenbacher, 2014; Domenech & Velankar, 2017). Such weakening of the gels was not measurable for oleogels prepared from large particles. For large particles, when the amount of added water exceeded 2.0 g/g, oil leaking was observed already while loading samples for rheological measurements, and further separation between particles and oil occurred during measurements; therefore, quantitative results could not be obtained for these samples. This particle separation was caused by the formation of dense agglomerates upon the addition of a critical amount of water, which were visible by eye. These dense agglomerates were not able to form a space-spanning network anymore, which eventually led to a collapse of the capillary suspension, i.e. of the gels' network structure.

We note here an important difference between oleogels with smaller and larger particles: Whereas water addition above a critical amount led to a collapse of the network in case of large particles, observed in the form of oil leaking, this was not the case for small particles. This can be explained by the larger surface area available in case of small particles, which enables network formation even upon extensive capillary bridge-induced clustering of the particles. However, a weakening of the network occurred at lower amounts of added water for small particles than for large particles, indicating that for small

particles, less secondary liquid was necessary to achieve a state of full bridge formation. This could be related to a smaller bridge volume and to increased pre-existing particle–particle contact already before the addition of water in case of small particles, which caused the point of oversaturation – and subsequent drop in G' – to be reached at a lower amount of added water.

Interestingly, the difference in G' between oleogels prepared from small and large particles of the same WAC decreased significantly upon water addition, and the maximum G' achieved was comparable for both particle types (Fig. 5a). Accordingly, the relative increase in G' was much larger for oleogels prepared from large particles, as shown in Fig. 5b. Based on previous research on oleogels prepared with silica (Koos et al., 2012) or glass beads (McCulfor, Himes, & Anklam, 2011), we expected the gel strength to be inversely related to the particle radius, meaning that gels prepared from smaller particles should have a higher G' over the whole range of added water. This expected influence of particle size held true for protein oleogels up to the maximum G', but not at higher amounts of added water. We attribute the large difference in relative increase of G' to differences in the initial gel strength of the systems without water. In the case of large particles, the initial gel was weak due to a low degree of particle interaction and limited surface area. Upon water addition, capillary bridge formation therefore led to a strong increase in particle interactions. In the case of small particles, particle interactions were already higher due to the larger surface area, and therefore the additional capillary bridges had a smaller effect. The more extensive network formation for small particles without added water was confirmed by a value of the loss tangent $\tan\delta$ of 0.16, which was much lower than the value of 0.34 found for large particles. The fact that the small particles did not reach a higher maximum G' than the large particles could further be related to traces of PGPR and mixing conditions. Especially for oleogels with small particles, for which more PGPR was used, remaining traces of PGPR may have weakened the capillary bridges by reducing the interfacial tension. In addition, for bridge formation, the added water needs to be broken up into droplets of a size below that of the particles (Dittmann & Willenbacher, 2014), which is more difficult to achieve for smaller particles, especially at higher amounts of added water, when the gels become increasingly thick.

Regarding the influence of WAC on G' upon water addition, the obtained results (Fig. 5) show that (1) contrary to our expectation, the plateau was reached at a comparable amount of added water for oleogels from particles with low and high WAC and (2) the effect of water addition was larger in case of high WAC-particles. In the case of particles with low WAC, less water can be absorbed by the particles, and therefore more water would be available to be used for capillary bridges. The plateau was thus expected to occur at a lower water content. Our unexpected result could be due to the fact that as suggested by the SESANS-results, a considerable amount of water likely stayed between the particles already at low amounts of added water, before the maximum WAC was reached. Therefore, a state of full bridge formation may had been obtained before differences in the maximum WAC begun to influence the amount of water remaining between the particles, and thus the gel strength. Furthermore, the variation in WAC between the particles was probably not sufficiently pronounced to easily detect differences in the amount of added water at which a maximum gel strength was obtained. Considering that differences in surface roughness between low and high WAC-particles were observed to have a large influence already for gels without water, it is likely that differences in surface roughness additionally obscured effects of WAC. In the case of particles with low WAC, where we would expect more water to be available for bridge formation and thus to increase gel strength, this effect is always counteracted by a higher surface roughness. For rougher surfaces, surface asperities need to be filled first, leaving less water available for bridge formation (Allard et al., 2022). As network structure (WAC) and surface roughness inherently vary together, preparation of particles with different WAC and similar roughness to separate both effects was not possible.

The much lower increase in G' for oleogels prepared from particles with low WAC can – similar to the observation for small particles – be attributed to a higher network connectivity already before the addition of water, which in this case is explained by a higher surface roughness of low WAC-particles as discussed above. However, also the maximum G' was slightly lower for low WAC-particles than for high WAC-particles. When comparing the maximum G' for particles of varying WAC, first the influence of differences in absorption ability and therefore differences in particle volume fraction upon water addition need to be considered. Based on the determined difference in WAC, the maximum variation in the particle volume for low and high WAC-particles is marginal (6%). Furthermore, as already discussed in context of the SESANS-results, the maximum amount of water added to the gels was much below the amount of water necessary to reach the maximum WAC. In addition, only part of this available water is located within the particles. Therefore, variations in the particle volume fraction of the oleogels due to variations in the particle volume depending on the particles' WAC are too small to explain the observed differences in gel strength. Thus, the obtained results indicate that upon addition of water, G' is dominated by the capillary force, which was lower in case of rougher surfaces. A first possible explanation is that in the case of low WAC-particles, particles were already more agglomerated before addition of water, due to the increased surface roughness. This would lead to a decreased surface area and thus to a lower number of bridges and a weaker gel upon water addition. However, if agglomerates were sufficiently stable to persist the process of water addition during sample preparation, these should have been visible in the PSD measurements (**Figure S3.2**, Supplementary Material), making this explanation less likely.

Thus, we attribute the observed effect of a lower maximum gel strength for rougher particles to the influence of roughness on the contact angle. An increased roughness often enhances hydrophobic surface properties of hydrophilic surfaces, which is reflected by an increase in contact angle, as found in experiments on nanoscale-roughness not only for inorganic surfaces (Müller, Riedel, Michel, De Paul, Hofer, Heger, & Grützmacher, 2001), but also for protein-containing polymer films (Jafari et al., 2015). Consequently, the increased contact angle results in a lower capillary force (see Eq. (1)) and a weaker gel. However, in recent work with silica particles, it was found that for comparable bridge volumes, gel strength was comparable for particles of different surface roughness, while the contact angle decreased with increasing roughness, which would provide an increase in capillary force (Allard et al., 2022). Such variations in the effect of surface roughness on the contact angle can explain deviating outcomes regarding the effect of surface roughness on network strength in different studies. The deviating results between studies also demonstrate that the effect of surface roughness on the capillary force is not easy to predict, which is not surprising considering that the influence of surface roughness on particle wettability is highly complex and depends on the specific physicochemical and structural properties of the surface (Ballard et al., 2019).

In conclusion, the presented gel strength results show that capillary suspension-based oleogels formed by spherical protein particles with water absorption and swelling capacity behave similarly as capillary suspensions prepared from more extensively studied inorganic particles. Upon water addition, gel strength initially increased rapidly, followed by a weakening of the network at higher amounts of added water. Smaller particles provided a higher gel strength for most of the range of added water, but at higher water contents, large particles reached a comparable gel strength. Regarding the influence of variations in WAC for the necessary amount of water to reach a maximum gel strength, our results suggest that concurrent variations of the surface roughness were more important, and dominated over potential effects of the differences in WAC. However, the effects of WAC are not clear from these results, likely attributed to the limited

difference in WAC for the utilized particles. Due to the obvious effect of WAC on the distribution of the water within and between particles, effects of WAC need to be verified by preparation of particles with larger differences in WAC in future research. Oleogels prepared from low WAC-particles had a higher gel strength than those with high WAC-particles of comparable size already before addition of water, which we attributed to the increased friction and contact in case of the rougher low WAC-particles. On the contrary, upon addition of water, gels prepared from low WAC-particles stayed somewhat below the gel strength reached for high WAC-particles, likely due to weaker capillary interactions caused by a larger contact angle for rougher particles. The obtained results show that even though similar maximum gel strengths were obtained, both particle size and surface roughness had a large influence on the range of changes in gel strength upon water addition, providing opportunities to adjust the material properties by controlling these particle properties.

3.4. Changes in network structure upon water addition

The above discussed results show that the network strength varies with the amount of added water and is influenced by different particle properties. To gain insight into the underlying network structure, CLSM images were taken for the systems with different water content (Fig. 6). For all oleogel types, before the addition of water, the network structures are relatively homogeneous. Already upon addition of a small amount of water (0.2 g/g), clustering of the protein particles is clearly observed, in agreement with the gel strength results. The networks are more contracted due to the formation of attractive capillary interactions, but no separate clusters are visible yet. When more water was added (0.4 g/g onwards), spherical agglomerates begin to form, which increase in size with further water addition. The clustering continues to such extent that the space-spanning network is disrupted, which explains the occurrence of oil leaking in case of the oleogels prepared from large particles with 2.4 g/g and 2.8 g/g added water, or the decrease in gel strength as observed for small particles.

Based on our CLSM images, the largest changes in network structure seem to appear at a water content up to 0.4 g/g for small particles, and 0.8 g/g for large particles. This matches the changes in the G'-curves, which show the most pronounced increase of G' for lower amounts of water addition. Regarding the maximum gel strength, the highest stability of capillary suspensions is expected in the funicular configuration (Bossler et al., 2018; Domenech & Velankar, 2015). This has indeed been found for capillary systems prepared with protein particles via ball-milling (Wang et al., 2022), but not for previously prepared protein systems via a solvent transfer (de Vries et al., 2018). In the latter work, the network structure seemed to have changed directly from funicular state clusters to a system where water droplets are stabilized by protein particles, i.e. a phase inversion occurred (de Vries et al., 2018). In our work, we observed yet another behavior: The maximum gel strength was reached at approximately 0.6 g/g and 1.2 g/g of added water for small and large particles, respectively. At these amounts of added water, the systems were clearly already in a state of spherical agglomeration, and therefore the gel strength would be expected to start decreasing.

Such unexpected occurrence of spherical agglomerates in absence of a decrease in network strength was also observed in Bossler's work (Bossler, 2018) on porous silica particles, and was attributed to the fact that the agglomerates may have become of similar size as the gap size in rheology experiments, which affected the measurements. However, in our research, the formation of spherical agglomerates occurred even before reaching a maximum G' not only in the case of large, but also for small protein particles. For small particles, the agglomerates appear to have a size below 100 μm, much below the gap size of 1 mm; thus, these results are not explained by possible inaccuracy of the measurements. The formation of spherical agglomerates is considered detrimental for the stability of capillary systems due to the immobilization of large amounts of secondary liquid, which is then not available to bridge single particles anymore (Bossler et al., 2017). We attribute the continuing increase or maintenance of G' with increasing water content for our systems to a still increasing connectivity through formation of additional capillary bridges between particles not yet incorporated in such spherical agglomerates. Network formation and thus gel strength is based on such a pendular network structure (Domenech & Velankar, 2014), which can still increase despite the fact that large spherical agglomerates, which do not contribute to the network, were already present.

This effect could be caused by the relatively mild mixing conditions, leading to inefficient droplet breakup and an uneven distribution of the water throughout the systems. Especially in case of the more solid-like samples, i.e. samples with higher amounts of added water, initial high local concentrations of water may have led to the formation of agglomerates, while more uniformly distributed water still contributed to additional network formation outside these clusters. The importance of mixing conditions and droplet breakup has been discussed in research on capillary systems prepared with silica particles and two immiscible polymers (Domenech & Velankar, 2014). The presence of large agglomerates was shown to strongly depend on the occurrence of large droplets of secondary liquid due to limited shear, leading to incorporation of the particles within these droplets. After formation of such agglomerates due to the presence of large secondary liquid droplets, as may be the case in the high water addition regime in this research, they are not broken down anymore during further shearing due to their high stability.

Comparing particles of high WAC varying in size, we observe that formation of large spherical agglomerates occurred at lower amounts of added water in the case of small particles. This is in agreement with gel strength results shown in Fig. 5, where a maximum gel strength was obtained at lower water addition for smaller particles, and also a drop in gel strength occurred earlier. An earlier transition from a pendular or funicular state to spherical agglomerates confirms that for small particles, liquid bridges started to merge already at lower amounts of added water, i.e., the critical bridge volume was lower.

For large particles with low WAC, large clusters seem to occur earlier than for large particles with high WAC (Fig. 6). Thus, while for the gel strength results (Fig. 5) differences in WAC were not clearly apparent, its effects on network structure may be more noticeable: If more water is available in between the particles due to a lower WAC, the critical bridge volume at which pendular bridges start to merge is reached at lower amounts of added water. We do not expect that this difference in network structure was caused by the influence of surface roughness, as from the gel strength results in the previous section, we concluded that the wetting angle was likely larger for the rougher low WAC-particles. If differences in contact angle were important for the point of network transition, merging of bridges and thus a transfer from pendular or funicular state to a state of spherical agglomeration would in case of a larger wetting angle, i.e. for rougher particles, theoretically be expected to occur at higher volume fractions of added water (Bossler, 2018; Miot et al., 2021), which is the opposite of what we observe. While we cannot draw firm conclusions due to the rather small difference in WAC between particles, this suggests that the point of network transition was determined by the volume of water available in between the particles, and thus related to differences in WAC. This would contrast with changes in gel strength, which were predominantly determined by differences in surface roughness and the subsequent differences in strength of the capillary force.

To gain more detailed insights into changes in the network structure upon water addition, we attempted to quantitatively analyze the CLSM images. We employed machine learning to identify the protein particles, which led to sufficiently reliable particle detection only for gels prepared with large particles of high WAC. For large particles of low WAC, the particle outlines were more irregular and particles were less distinguishable. For small particles, their size was too small to detect

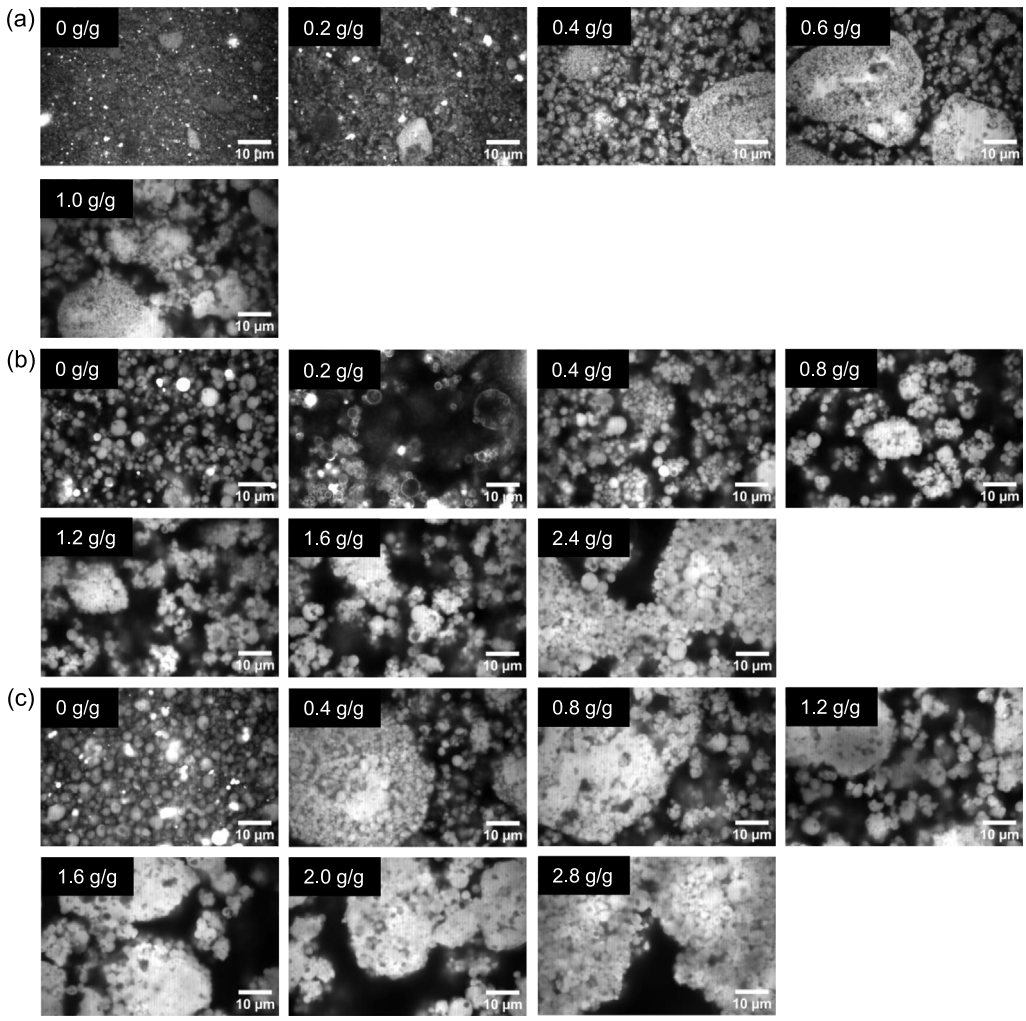

Fig. 6. CLSM images of protein oleogels prepared from (a) small particles, high WAC, (b) large particles, high WAC and (c) large particles, low WAC with increasing amount of added water.

individual particles. Fig. 7 shows the number of nearest neighbors, N, average nearest particle distance, D, and Hopkins statistics, H, for oleogels prepared from large particles with high WAC for all water additions. The Hopkins statistics, H, describes the degree of clustering, for which a value of 0 indicates a uniform distribution, while a value of 1 signifies strong clustering (Pierna & Massart, 2000). The data points for oleogels with 0.2 g/g were omitted from the data set, due to insufficiently accurate detection of the particles at this water content.

For all three parameters, the expected trends are visible: The amount of nearest neighbors increased with increasing water addition, the particle distance decreased and the Hopkins parameter, H, increased, confirming the development of a more interconnected structure. Whereas H increased in a rather continuous fashion, for N and D, the largest difference in values occurred between 0 g/g and 0.4 g/g of added water, which matches the large increase in G' in this range (Fig. 5). This implies that the mechanical strength of the gels is highly influenced by the number of connections and the proximity of the particles in this water concentration range. At higher amounts of added water, despite the plateau in G' obtained for the large particles, these parameters confirm that the structure and organization of the gel networks indeed evolved further, i.e. agglomeration of the particles continued. This aligns with the eventual oil leakage of the gels at the highest amount of added water, and the observed continuing changes in their morphological appearance as shown in Fig. 1. That the increase in H was not as pronounced in the lower water addition range as in the case of N and D is likely because H provides a more global perspective on clustering tendency. Thus, even if particles started to get closer on a local scale, as indicated by N and D, their global distribution was still rather uniform.

While we could not perform quantitative image analysis for oleogels prepared with small particles, we have access on information on their spatial arrangement through SESANS, as described in Section 3.2. As already mentioned, only small particles were within the length scale of the SESANS-technique (Bouwman, 2021). Next to the scattering length density (Section 3.2), we also determined the fractal dimension, D_f, by fitting the scattering data to a fractal model (Fig. 2a, methods Section 2.2.8). The obtained values for D_f are shown in Fig. 8 and provide similar information as the parameters obtained from image analysis. Due to the limited length scale of one order of magnitude over which the network structure was observed (particle size of ~ 1 µm, maximum length scale accessible by SESANS ~ 20 µm (Bouwman, 2021)) the values for the fractal dimension may not represent an accurate description of the fractal nature of the gel's network structure. Nevertheless, a larger value for the fractal dimension can be interpreted as a higher compactness of the aggregate clusters (Nieuwland, Bouwman, Pouvreau, Martin, & de Jongh, 2016), enabling a quantitative comparison of the network structures between gels with varying amounts of added water. As expected, given the changes of N, D and H for large particles, D_f increased with the addition of water, from 1.3 up to a maximum value of 2.5. The largest difference in D_f was obtained between 0.2 and 0.4 g/g of added water. This is consistent with the large degree of structural changes observed in the CLSM images, suggesting a transition

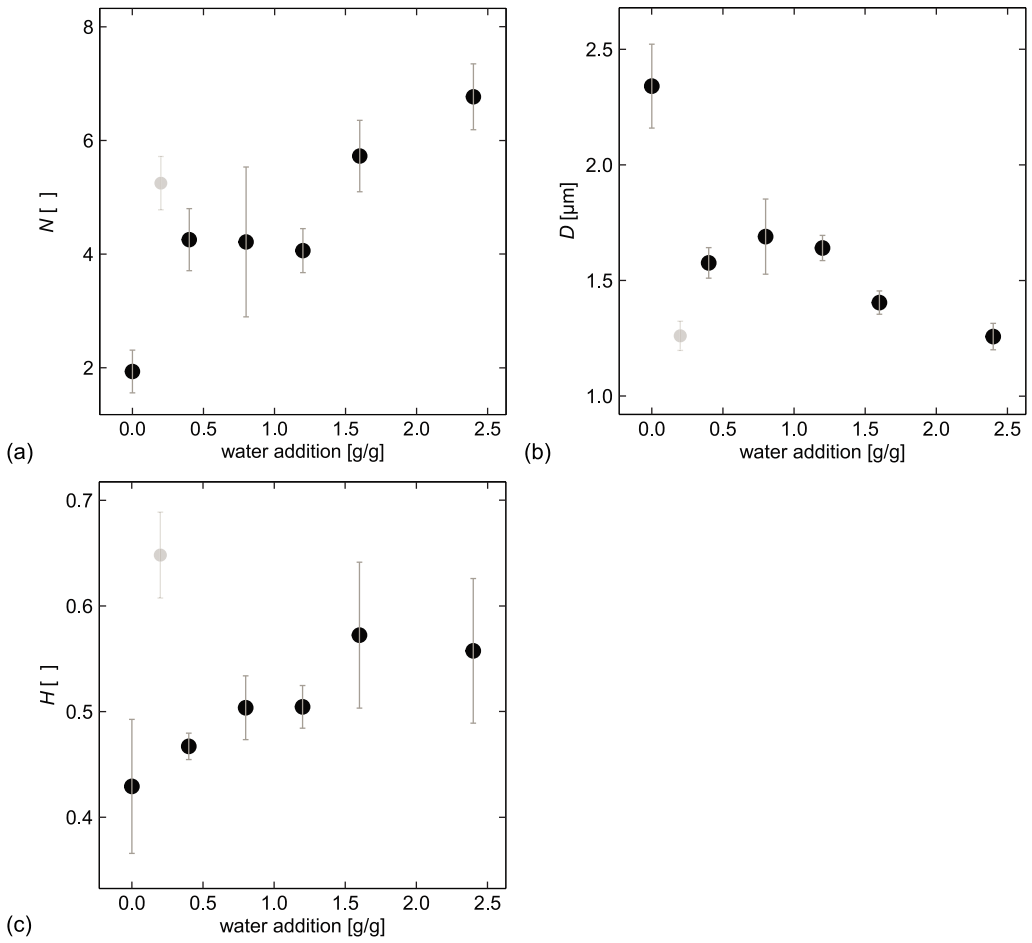

Fig. 7. (a) Number of neighboring particles, *N*, (b) average nearest particle distance, *D*, and (c) Hopkins statistic, *H*, for oleogels prepared from large particles at high WAC. Error bars indicate standard deviations obtained from analysis of minimally 17 images.

from a pendular or funicular state to a spherical agglomeration state.

Overall, changes in network structure visible from CLSM images show that the networks transitioned from a pendular/funicular state to a state of spherical agglomeration, which has also been observed for particles of synthetic origin. Quantitative analysis from imaging and scattering techniques confirmed that as more water is added, the particles cluster more. While the pronounced increase of the determined clustering parameters in the low water range matched the initial fast increase in gel strength, the maximum gel strengths were – against expectations from theory and results from synthetic particles – reached after a state at which spherical agglomeration already occurred. Such transition in the network structure was obtained at lower amount of water for smaller particles, pointing to an overall smaller available bridge volume for small particles. Regarding WAC, low WAC-particles seem to cluster more extensively already at lower amounts of added water, as expected for particles that absorb less water. This suggests that changes in network configuration are mainly determined by the volume of secondary liquid located between the particles, i.e. by differences in WAC, whereas gel strength is determined by the strength of attractive interactions, for which other properties such as surface roughness are more important.

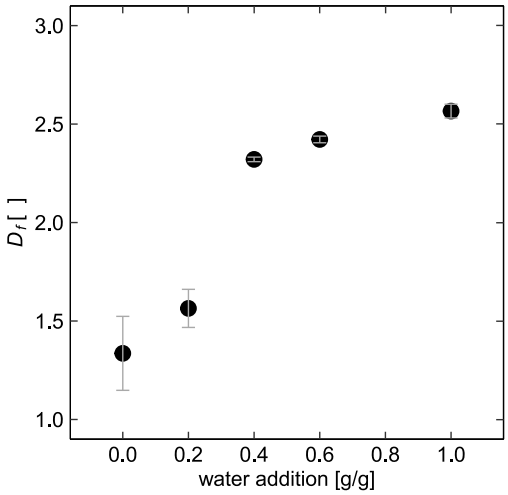

Fig. 8. Fractal dimensions, D_f, of oleogels prepared with small particles at increasing amount of added water, determined from the in duplicate performed SESANS-measurements.

4. Conclusion

By preparing protein particles, designed to vary in size and water absorption capacity (WAC), we were able to gain insights into the effect of different particle properties on the gel strength and structural behavior of biopolymer-based capillary suspensions. The effect of particle size depended strongly on the amount of water added. When no water was added, gels prepared from smaller particles already had a higher gel strength, due to the higher total surface area compared to larger particles. At intermediate water content, a comparable maximum gel strength was obtained for both particle sizes. However, as for small particles the network transitioned from a pendular or funicular

state to a state of spherical agglomeration at lower water content, this maximum strength and subsequent weakening of the gels with increasing water content occurred earlier for smaller particles. The agglomeration-induced occurrence of oil leakage at high water content, which was observed only for large particles, indicated the critical role of particle size for the availability of sufficient surface area for maintained network formation upon particle clustering.

In addition, variations in WAC were expected to directly influence gel strength due to their impact on the water distribution, but this effect was not observed. Instead, the effect of concurrent variations in surface roughness was dominant. Variations in surface roughness led to even more pronounced differences in initial gel strength than variations in particle size, and thus also to larger differences in the relative increase in gel strength when water was added. In addition, for a higher degree of surface roughness, a slightly lower maximum gel strength was obtained, most likely due to changes in the contact angle, which in turn affects the capillary force. However, differences in WAC, and thus a larger amount of secondary liquid available for bridge formation in case of low WAC-particles, appeared to reflect in a slightly earlier transition to a state of spherical agglomeration for these particles. As the difference in WAC was limited for our particles, future research could verify these effects by using particles with a wider range of absorption ability.

Overall, we show that oleogels in the form of capillary suspensions could be prepared with spherical, highly absorbing biopolymeric particles. We succeeded to also visually demonstrate that water-absorbing particles still contain water bridges between them, and conclude from results obtained by the SESANS-technique that water was located also between the particles already at the lowest amounts of added water. We further show that the range of gel strengths obtained for such materials upon water addition can be easily tuned by varying different particle characteristics, such as size and surface roughness. These findings provide opportunities for the design of new food and pharmaceutical materials with specific desired characteristics.

CRediT authorship contribution statement

Annika Feichtinger: Writing – original draft, Visualization, Methodology, Investigation, Formal analysis, Conceptualization. **Ahmed Jarray:** Writing – review & editing, Methodology, Formal analysis. **Wim G. Bouwman:** Writing – review & editing, Resources, Methodology, Formal analysis. **Chris P. Duif:** Methodology, Investigation, Formal analysis. **Maria C. Valverde-Ayllon:** Methodology, Investigation. **Karlijn Heerkens:** Writing – review & editing, Methodology, Investigation. **Renee Rooijakkers:** Methodology, Investigation. **Jasper Landman:** Writing – review & editing, Supervision, Methodology, Conceptualization. **Elke Scholten:** Writing – review & editing, Supervision, Project administration, Methodology, Funding acquisition, Conceptualization.

Declaration of competing interest

The authors declare that they have no known competing financial interests or personal relationships that could have appeared to influence the work reported in this paper.

Acknowledgments

This publication is part of the project “Protein oleogels: capillary suspensions as a novel approach to control protein network formation and rheological behaviour” (with project number 712.018.002) of the research program NWO-ECHO, which is financed by the Dutch Research Council (NWO). This work benefited from the use of the SasView application, originally developed under NSF award DMR-0520547. SasView contains code developed with funding from the European Union’s Horizon 2020 research and innovation program under the SINE2020 project, grant agreement No 654000. We thank the Reactor Institute of the Delft University of Technology for providing beam time for the SESANS measurements.

Appendix A. Supplementary data

Supplementary material related to this article can be found online at https://doi.org/10.1016/j.foodhyd.2025.111061.

Data availability

Data will be made available on request.

References

Allard, J., Burgers, S., González, M. C. R., Zhu, Y., De Feyter, S., & Koos, E. (2022). Effects of particle roughness on the rheology and structure of capillary suspensions. *Colloids and Surfaces A*, *648*, Article 129224. http://dx.doi.org/10.1016/j.colsurfa.2022.129224.

Bakker, J. H., Washington, A. L., Parnell, S. R., van Well, A. A., Pappas, C., & Bouwman, W. G. (2020). Analysis of SESANS data by numerical Hankel transform implementation in SasView. *Journal of Neutron Research*, *22*, 57. http://dx.doi.org/10.3233/jnr-200154.

Ballard, N., Law, A. D., & Bon, S. A. (2019). Colloidal particles at fluid interfaces: Behaviour of isolated particles. *Soft Matter*, *15*, 1186. http://dx.doi.org/10.1039/c8sm02048e.

Banerjee, A., & Dave, R. (2004). Validating clusters using the Hopkins statistic. In *2004 IEEE International Conference on Fuzzy Systems (IEEE cat. no.04CH37542)*: *vol. 1*, (p. 149). http://dx.doi.org/10.1109/FUZZY.2004.1375706.

Berg, S., Kutra, D., Kroeger, T., Straehle, C. N., Kausler, B. X., Haubold, C., et al. (2019). Ilastik: Interactive machine learning for (bio)image analysis. *Nature Methods*, *16*, 1226. http://dx.doi.org/10.1038/s41592-019-0582-9.

Bindgen, S., Allard, J., & Koos, E. (2022). The behavior of capillary suspensions at diverse length scales: From single capillary bridges to bulk. *Current Opinion in Colloid & Interface Science*, *58*, Article 101557. http://dx.doi.org/10.1016/j.cocis.2021.101557.

Bossler, F. (2018). *Structural investigations of capillary suspensions using rheology and confocal microscopy* (Ph.D. thesis), Karlsruher Institut für Technologie (KIT), http://dx.doi.org/10.5445/IR/1000084157.

Bossler, F., & Koos, E. (2016). Structure of particle networks in capillary suspensions with wetting and nonwetting fluids. *Langmuir*, *32*, 1489. http://dx.doi.org/10.1021/acs.langmuir.5b04246.

Bossler, F., Maurath, J., Dyhr, K., Willenbacher, N., & Koos, E. (2018). Fractal approaches to characterize the structure of capillary suspensions using rheology and confocal microscopy. *Journal of Rheology*, *62*, 183. http://dx.doi.org/10.1122/1.4997889.

Bossler, F., Weyrauch, L., Schmidt, R., & Koos, E. (2017). Influence of mixing conditions on the rheological properties and structure of capillary suspensions. *Colloids and Surfaces A*, *518*, 85. http://dx.doi.org/10.1016/j.colsurfa.2017.01.026.

Bouwman, W. G. (2021). Spin-echo small-angle neutron scattering for multiscale structure analysis of food materials. *Food Structure*, *30*, Article 100235. http://dx.doi.org/10.1016/j.foostr.2021.100235.

de Vries, A. (2017). *Structuring oil by protein building blocks* (Ph.D. thesis), Wageningen University and Research, http://dx.doi.org/10.18174/403635.

de Vries, A., Jansen, D., van der Linden, E., & Scholten, E. (2018). Tuning the rheological properties of protein-based oleogels by water addition and heat treatment. *Food Hydrocolloids*, *79*, 100. http://dx.doi.org/10.1016/j.foodhyd.2017.11.043.

de Vries, A., Wesseling, A., van der Linden, E., & Scholten, E. (2017). Protein oleogels from heat-set whey protein aggregates. *Journal of Colloid and Interface Science*, *486*, 75. http://dx.doi.org/10.1016/j.jcis.2016.09.043.

Dittmann, J., & Willenbacher, N. (2014). Micro structural investigations and mechanical properties of macro porous ceramic materials from capillary suspensions. *Journal of the American Ceramic Society*, *97*, 3787. http://dx.doi.org/10.1111/jace.13184.

Domenech, T., & Velankar, S. (2014). Capillary-driven percolating networks in ternary blends of immiscible polymers and silica particles. *Rheologica Acta*, *53*, 593. http://dx.doi.org/10.1007/s00397-014-0776-0.

Domenech, T., & Velankar, S. S. (2015). On the rheology of pendular gels and morphological developments in paste-like ternary systems based on capillary attraction. *Soft Matter*, *11*, 1500. http://dx.doi.org/10.1039/C4SM02053G.

Domenech, T., & Velankar, S. S. (2017). Microstructure, phase inversion and yielding in immiscible polymer blends with selectively wetting silica particles. *Journal of Rheology*, *61*, 363. http://dx.doi.org/10.1122/1.4975931.

Feichtinger, A., Groot Nibbelink, D., Poppe, S., Bozzo, L., Landman, J., & Scholten, E. (2022). Protein oleogels prepared by solvent transfer method with varying protein sources. *Food Hydrocolloids*, *132*, Article 107821. http://dx.doi.org/10.1016/j.foodhyd.2022.107821.

Fuhrmann, P. L., Powell, J., & Rousseau, D. (2023). Structure and rheology of oil-continuous capillary suspensions containing water-swellable cellulose beads and fibres. *Food Hydrocolloids*, *139*, Article 108503. http://dx.doi.org/10.1016/j.foodhyd.2023.108503.

Fysun, O., Nöbel, S., Loewen, A. J., & Hinrichs, J. (2018). Tailoring yield stress and viscosity of concentrated microgel suspensions by means of adding immiscible liquids. *LWT–Food Sci. Technol.*, *93*, 51. http://dx.doi.org/10.1016/j.lwt.2018.03.013.

Gao, Z., Zhang, C., Li, Y., Wu, Y., Deng, Q., & Ni, X. (2023). Edible oleogels fabricated by dispersing cellulose particles in oil phase: Effects from the water addition. *Food Hydrocolloids*, *134*, Article 108040. http://dx.doi.org/10.1016/j.foodhyd.2022.108040.

Guinier, A., Fournet, G., Walker, C. B., & Yudowitch, K. L. (1955). *Small-angle scattering of X-rays*. Wiley New York.

Hoffmann, S., Koos, E., & Willenbacher, N. (2014). Using capillary bridges to tune stability and flow behavior of food suspensions. *Food Hydrocolloids*, *40*, 44. http://dx.doi.org/10.1016/j.foodhyd.2014.01.027.

Jafari, S. M., Khanzadi, M., Mirzaei, H., Dehnad, D., Chegini, F. K., & Maghsoudlou, Y. (2015). Hydrophobicity, thermal and micro-structural properties of whey protein concentrate–pullulan–beeswax films. *International Journal of Biological Macromolecules*, *80*, 506. http://dx.doi.org/10.1016/j.ijbiomac.2015.07.017.

Jain, A. K., & Dubes, R. C. (1988). *Algorithms for clustering data*. Prentice-Hall, Inc.

Jarray, A., Feichtinger, A., & Scholten, E. (2022). Linking intermolecular interactions and rheological behaviour in capillary suspensions. *Journal of Colloid and Interface Science*, *627*, 415. http://dx.doi.org/10.1007/s00396-020-04772-8.

Koos, E. (2014). Capillary suspensions: Particle networks formed through the capillary force. *Current Opinion in Colloid & Interface Science*, *19*, 575. http://dx.doi.org/10.1016/j.cocis.2014.10.004.

Koos, E., Johannsmeier, J., Schwebler, L., & Willenbacher, N. (2012). Tuning suspension rheology using capillary forces. *Soft Matter*, *8*, 6620. http://dx.doi.org/10.1039/c2sm25681a.

Koos, E., & Willenbacher, N. (2011). Capillary forces in suspension rheology. *Science*, *331*, 897. http://dx.doi.org/10.1126/science.1199243.

Lam, R. S., & Nickerson, M. T. (2015). The effect of pH and temperature pretreatments on the physicochemical and emulsifying properties of whey protein isolate. *LWT–Food Science & Technology*, *60*, 427. http://dx.doi.org/10.1016/j.lwt.2014.07.031.

Li, Y., Zhang, C., Hu, B., Gao, Z., Wu, Y., Deng, Q., et al. (2023). Formation and application of edible oleogels prepared by dispersing soy fiber particles in oil phase. *Food Research International*, *164*, Article 112369. http://dx.doi.org/10.1016/j.foodres.2022.112369.

Manzoor, S., Masoodi, F., Naqash, F., & Rashid, R. (2022). Oleogels: Promising alternatives to solid fats for food applications. *Food Hydrocolloids Health*, *2*, Article 100058. http://dx.doi.org/10.1016/j.fhfh.2022.100058.

Maubois, J.-L., & Lorient, D. (2016). Dairy proteins and soy proteins in infant foods nitrogen-to-protein conversion factors. *Dairy Sci. Technol.*, *96*, 15. http://dx.doi.org/10.1007/s13594-015-0271-0.

McCulfor, J., Himes, P., & Anklam, M. R. (2011). The effects of capillary forces on the flow properties of glass particle suspensions in mineral oil. *AIChE Journal*, *57*, 2334. http://dx.doi.org/10.1002/aic.12451.

McMeekin, T. L., Groves, M. L., & Hipp, N. J. (1964). Refractive indices of amino acids, proteins, and related substances. In *Amino Acids and Serum Proteins* (pp. 54–66). ACS Publications, http://dx.doi.org/10.1021/ba-1964-0044.ch004.

Miot, M., Veylon, G., Wautier, A., Philippe, P., Nicot, F., & Jamin, F. (2021). Numerical analysis of capillary bridges and coalescence in a triplet of spheres. *Granular Matter*, *23*, 65. http://dx.doi.org/10.1007/s10035-021-01127-0.

Müller, F. J., Isa, L., & Vermant, J. (2023). Toughening colloidal gels using rough building blocks. *Nature Communications*, *14*, 5309. http://dx.doi.org/10.1038/s41467-023-41098-9.

Müller, B., Riedel, M., Michel, R., De Paul, S. M., Hofer, R., Heger, D., et al. (2001). Impact of nanometer-scale roughness on contact-angle hysteresis and globulin adsorption. *Journal of Vacuum Science & Technology B: Microelectronics and Nanometer Structures–Processing, Measurement, and Phenomena*, *19*, 1715. http://dx.doi.org/10.1116/1.1392402.

Nguyen, H. N. G., Zhao, C.-F., Millet, O., & Selvadurai, A. (2021). Effects of surface roughness on liquid bridge capillarity and droplet wetting. *Powder Technology*, *378*, 487. http://dx.doi.org/10.1016/j.powtec.2020.10.016.

Nicolai, T., & Durand, D. (2013). Controlled food protein aggregation for new functionality. *Current Opinion in Colloid & Interface Science*, *18*, 249. http://dx.doi.org/10.1016/j.cocis.2013.03.001.

Nieuwland, M., Bouwman, W. G., Pouvreau, L., Martin, A. H., & de Jongh, H. H. (2016). Relating water holding of ovalbumin gels to aggregate structure. *Food Hydrocolloids*, *52*, 87. http://dx.doi.org/10.1016/j.foodhyd.2015.06.018.

NIST IGOR/DANSE (2014). SasView 5.0.6 documentation, sphere functions, sphere. URL: https://www.sasview.org/docs/user/models/sphere.html. (Accessed 10 November 2023).

NIST IGOR/DANSE (2017). SasView 5.0.6 documentation, shape-independent functions, fractal. URL: https://www.sasview.org/docs/user/models/fractal.html. (Accessed 10 November 2023).

Pierna, J. F., & Massart, D. (2000). Improved algorithm for clustering tendency. *Analytica Chimica Acta*, *408*, 13. http://dx.doi.org/10.1016/S0003-2670(99)00879-X.

Pirozzi, A., & Donsì, F. (2023). Structuring vegetable oils through the formation of capillary suspensions: Comparison of wheat middlings and pure cellulose processed by high-pressure homogenization. *Chemical Engineering Transactions*, *102*, 151. http://dx.doi.org/10.3303/CET23102026.

Pirozzi, A., Posocco, A., & Donsì, F. (2023). Oil structuring through capillary suspensions prepared with wheat middlings micronized directly in oil by high-pressure homogenization. *Food Hydrocolloids*, *145*, Article 109152. http://dx.doi.org/10.1016/j.foodhyd.2023.109152.

Plazzotta, S., Calligaris, S., & Manzocco, L. (2020). Structural characterization of oleogels from whey protein aerogel particles. *Food Research International*, *132*, Article 109099. http://dx.doi.org/10.1016/j.foodres.2020.109099.

Quillin, M. L., & Matthews, B. W. (2000). Accurate calculation of the density of proteins. *Acta Crystallographica. Section D: Biological Crystallography*, *56*, 791. http://dx.doi.org/10.1107/s090744490000679x.

Ranquet, O., Duce, C., Bramanti, E., Dietemann, P., Bonaduce, I., & Willenbacher, N. (2023). A holistic view on the role of egg yolk in Old Masters' oil paints. *Nature Communications*, *14*, 1. http://dx.doi.org/10.1038/s41467-023-36859-5.

Rekveldt, M. T., Plomp, J., Bouwman, W. G., Kraan, W. H., Grigoriev, S., & Blaauw, M. (2005). Spin-echo small angle neutron scattering in Delft. *Review of Scientific Instruments*, *76*(3), http://dx.doi.org/10.1063/1.1858579.

Sağlam, D., Venema, P., de Vries, R., van Aelst, A., & van der Linden, E. (2012). Relation between gelation conditions and the physical properties of whey protein particles. *Langmuir*, *28*, 6551. http://dx.doi.org/10.1021/la300344g.

Sağlam, D., Venema, P., de Vries, R., Sagis, L. M., & van der Linden, E. (2011). Preparation of high protein micro-particles using two-step emulsification. *Food Hydrocolloids*, *25*, 1139. http://dx.doi.org/10.1016/j.foodhyd.2010.10.011.

Sasview (2022). URL: https://www.sasview.org/. Version 5.0.5.

Teixeira, J. (1988). Small-angle scattering by fractal systems. *Journal of Applied Crystallography*, *21*, 781. http://dx.doi.org/10.1107/S0021889888000263.

Wang, G.-S., Chen, H.-Y., Wang, L.-J., Zou, Y., Wan, Z.-L., & Yang, X.-Q. (2022). Formation of protein oleogels via capillary attraction of engineered protein particles. *Food Hydrocolloids*, *133*, Article 107912. http://dx.doi.org/10.1016/j.foodhyd.2022.107912.

Wilson, H. J., & Davis, R. H. (2000). The viscosity of a dilute suspension of rough spheres. *Journal of Fluid Mechanics*, *421*, 339. http://dx.doi.org/10.1017/S0022112000001695.

Zhang, Z., Arrighi, V., Campbell, L., Lonchamp, J., & Euston, S. R. (2016). Properties of partially denatured whey protein products 2: Solution flow properties. *Food Hydrocolloids*, *56*, 218. http://dx.doi.org/10.1016/j.foodhyd.2015.12.012.